

X-RAY CONSTRAINTS ON THE LOCAL SUPERMASSIVE BLACK HOLE OCCUPATION FRACTION

BRENDAN P. MILLER,^{1,2} ELENA GALLO,¹ JENNY E. GREENE,³ BRANDON C. KELLY,⁴ TOMMASO TREU,⁴ JONG-HAK WOO⁵,
& VIVIENNE BALDASSARE¹

Draft version October 24, 2014

ABSTRACT

Distinct seed formation mechanisms are imprinted upon the fraction of dwarf galaxies currently containing a central supermassive black hole. Seeding by Pop III remnants is expected to produce a higher occupation fraction than is generated with direct gas collapse precursors. *Chandra* observations of nearby early-type galaxies can directly detect even low-level supermassive black hole activity, and the active fraction immediately provides a firm lower limit to the occupation fraction. Here, we use the volume-limited AMUSE surveys of ~ 200 optically-selected early-type galaxies to characterize simultaneously, for the first time, the occupation fraction and the scaling of L_X with M_{star} , accounting for intrinsic scatter, measurement uncertainties, and X-ray limits. For early-type galaxies with $M_{\text{star}} < 10^{10} M_\odot$, we obtain a lower limit to the occupation fraction of $>20\%$ (at 95% confidence), but full occupation cannot be excluded. The preferred dependence of $\log L_X$ upon $\log M_{\text{star}}$ has a slope of $\sim 0.7\text{--}0.8$, consistent with the “downsizing” trend previously identified from the AMUSE dataset, and a uniform Eddington efficiency is disfavored at $\sim 2\sigma$. We provide guidelines for the future precision with which these parameters may be refined with larger or more sensitive samples.

Subject headings: black hole physics — galaxies: nuclei

1. INTRODUCTION

Observations of high-redshift quasars indicate that supermassive black holes (SMBHs⁶) are already present in the early universe (e.g., Vestergaard & Osmer 2009; Willott et al. 2010; Mortlock et al. 2011). SMBHs with $M_{\text{BH}} \gtrsim 10^9 M_\odot$ by $z \gtrsim 6$ are extremely challenging to grow from Population III remnants (“light” seeds of $\sim 100 M_\odot$; e.g., Whalen & Fryer 2012; Madau et al. 2014; Taylor & Kobayashi 2014), but can derive from direct gas collapse precursors (“heavy” seeds of $\sim 10^5 M_\odot$; e.g., Begelman 2010; Johnson et al. 2013; Ferrara et al. 2014). However, the unresolved cosmic X-ray background implies SMBHs are not common (or else are generally quasi-quiescent) in high-redshift galaxies (Salvaterra et al. 2012), a possibility also suggested by stringent constraints on average nuclear X-ray luminosities obtained from stacking deep field *Chandra* observations (Triester et al. 2013). For typical expected subsequent black hole growth (Shankar et al. 2013), and in line with the SMBH mass function derived from broad-line quasars (Natarajan & Volonteri 2012), these results may be more consistent with sparse heavy seeding than with slow initial growth of omnipresent light seeds. Despite significant and ongoing theoretical and observational advances, the particular seed mechanism predominantly responsible for SMBH formation is not yet conclusively established (see reviews

by Volonteri 2012; Volonteri & Bellovary 2012; Natarajan 2014; and references therein).

The evolution of SMBHs appears to be entwined with that of their host galaxies. This is suggested by the $M_{\text{BH}} - \sigma$ relation linking the central black hole mass to the bulge stellar velocity dispersion, which holds for both quiescent spheroids (Gültekin et al. 2009; McConnell & Ma 2013) and active galactic nuclei (Woo et al. 2010, 2013) and may be redshift-dependent (Treu et al. 2007; Lapi et al. 2014). SMBH feedback provides one plausible linking mechanism (Sun et al. 2013), as predicted by semi-empirical modeling (Croton et al. 2006; Shankar et al. 2013) and in a few cases now directly measured (e.g., Feruglio et al. 2010; Cano-Díaz et al. 2012; Liu et al. 2013). Mergers and intermittently efficient accretion in larger SMBHs spur growth and remove observational signatures of their birth, but smaller SMBHs have more subdued histories and undergo mostly secular evolution (Jiang et al. 2011). Consequently, both the mass distribution and the very rate of occurrence of SMBHs in lower-mass galaxies contain archaeological information on the initial seed formation mechanism.

A robust conclusion from semi-analytical modeling is that smaller galaxies are more likely to contain SMBHs when Pop III remnants, rather than direct gas collapse, provide the dominant⁷ seeding mode (Volonteri & Natarajan 2009; Volonteri 2010; van Wassenhove et al. 2010). This is because cold low-metallicity gas is only able to collapse to a central massive object in halos with low spin parameter, otherwise disk fragmentation leads to star formation (van Wassenhove et al. 2010). The fraction of halos forming such heavy seeds should exceed 0.001 to produce SMBHs at $z = 6 - 7$ (Petri et al. 2012). Using a First Billion Years cosmological hydrodynamical simulation, Agarwal et al. (2014) identify

¹ Department of Astronomy, University of Michigan, Ann Arbor, MI 48109, USA

² Department of Physics and Astronomy, Macalester College, Saint Paul, MN 55105, USA

³ Department of Astrophysics, Princeton University, Princeton, NJ 08544, USA

⁴ Physics Department, University of California, Santa Barbara, CA 93106, USA

⁵ Astronomy Program, Department of Physics and Astronomy, Seoul National University, Seoul, Korea

⁶ We use the term “supermassive” to indicate masses of $M_{\text{BH}} \gtrsim 3 \times 10^5 M_\odot$ for central black holes, as in Greene (2012).

⁷ Intermediate mass seeds, for example from nuclear star cluster collapse (Davies et al. 2011; Lupi et al. 2014), are a third possibility.

several pristine⁸ atomic-cooling haloes that could host direct-collapse massive seeds, and note that these haloes are universally close to protogalaxies and exposed to a high flux of Lyman-Werner radiation (as also found by, e.g., Latif et al. 2013a, b; Dijkstra et al. 2014). Measurement of the occupation fraction (i.e., the percentage of galaxies hosting SMBHs) in nearby galaxies, particularly at low stellar masses $M_{\text{star}} < 10^{9-10} M_{\odot}$, is an effective *observational* discriminator between light versus heavy seeds (Greene 2012).

The limited $\lesssim 10^8$ yr lifetime of luminous quasars suggests (Soltan 1982; Yu & Tremaine 2002), consistent with observations, that the most massive “inactive” galaxies invariably host SMBHs now accreting/radiating only at $\lesssim 10^{-5}$ Eddington, but the occupation fraction in lower mass galaxies remains uncertain. Clearly some low-mass galaxies do possess SMBHs⁹, even active ones. For example, the dwarf galaxy Henize 2-10 hosts an accreting SMBH as revealed by X-ray and radio emission (Reines et al. 2011), and features central blue clumps of star-formation within a red early-type system (Nguyen et al. 2014). Mrk 709 is an interacting pair of dwarfs, the Southern of which has a central X-ray and radio source indicating the presence of a SMBH (Reines et al. 2014). Within the *Chandra* Deep Field South Survey, Schramm et al. (2013) identify three galaxies with $M_{\star} < 3 \times 10^9 M_{\odot}$ that have X-ray emitting SMBHs. Yuan et al. (2014) describe four dwarf Seyferts with $M_{\text{BH}} \lesssim 10^6 M_{\odot}$, two of which are detected in X-rays with $L_X \sim 10^{41} \text{ erg s}^{-1}$. A sample of 151 dwarf galaxies with candidate SMBHs as identified from optical emission line ratios and/or broad H α emission is presented by Reines et al. (2013; see also references therein). The ultra-compact dwarf galaxy M60-UCD1 is indicated by a central velocity dispersion peak to have a SMBH with $M_{\text{BH}} = 2.1 \times 10^7 M_{\odot}$, but here the large black hole mass fraction suggests substantial stellar mass has been stripped from the galaxy (Seth et al. 2014). For each example of a low-mass galaxy that has observational evidence for a central SMBH, there are 10–100 similar galaxies for which the presence or absence of a black hole is currently impossible to measure. However, dynamical mass constraints are quite stringent for some Local Group objects (the spiral M33: Gebhardt et al. 2001; Merritt et al. 2001; the dwarf elliptical NGC 205: Valluri et al. 2005), which effectively rules out a 100% SMBH occupation fraction.

High spatial resolution X-ray observations can efficiently identify very low-level SMBH activity (Soria et al. 2006; Pellegrini 2010) without contamination from the stellar emission that dilutes optical searches. Nuclear X-ray emission directly measures high-energy accretion-linked radiative output and additionally serves as a plausible proxy for mechanical feedback (Allen et al. 2006; Balmaverde et al. 2008). X-ray studies of low-level SMBH activity are best conducted on galaxies with low star formation rates to eliminate potential contamination from high-mass X-ray binaries. For statistical purposes the sample must span a wide range in M_{star} and be

unbiased with respect to optical or X-ray nuclear properties. These criteria are satisfied by the AMUSE¹⁰-Virgo (Gallo et al. 2008, 2010; G08, G10 hereafter) and AMUSE-Field (Miller et al. 2012a, 2012b; M12a, M12b hereafter) surveys, which are Large *Chandra* Programs that together targeted 203 optically-selected early-type galaxies at $d < 30$ Mpc, and now include *HST*, *Spitzer*, and *VLA/JVLA* coverage. Almost all of these galaxies have $L_X < 10^{41} \text{ erg s}^{-1}$ and $L_X/L_{\text{Edd}} < 10^{-5}$, below limits commonly used to distinguish active galactic nuclei (AGN) from “inactive” galaxies.

In this work we use the AMUSE dataset to obtain the first simultaneous constraints upon the scaling of nuclear activity with host galaxy stellar mass and the local super-massive black hole occupation fraction, and derive guidelines for the precision that may be achieved with a larger sample or a next-generation X-ray telescope.

2. DISENTANGLING OCCUPATION AND DOWNSIZING

The AMUSE nuclear detection fractions constitute, after correcting for potential minor low-mass X-ray binary contamination (G08; G10; M12a), strict lower limits on the occupation fraction. Taking as given that all higher-mass early-type galaxies host SMBHs, the efficiency with which their nuclear X-ray sources are found suggests a correction factor to apply to the lower-mass galaxies. After assuming a uniform distribution of Eddington-scaled luminosity, the occupation fraction can be calculated in a straightforward fashion by imposing a limiting Eddington sensitivity threshold. This approach tentatively favors heavy seeds (Greene 2012).

However, the assumption of a mass-independent Eddington ratio distribution is disfavored by the data. Both the Virgo and Field galaxies display an apparent “downsizing” trend (with a consistent slope) toward relatively greater Eddington-scaled X-ray luminosity in lower-mass galaxies or for inferred lower-mass SMBHs (G10; M12a; M12b). While this downsizing tendency is qualitatively similar to the effect found at higher masses and accretion rates for quasars, the physical explanation may be completely distinct, given the very low accretion rates and radiative efficiencies that characterize the AMUSE sample (including M 87, which has a mass accretion rate directly constrained by the rotation measure to be two orders of magnitude below Bondi; Kuo et al. 2014). Thus, we cannot make direct comparisons with recent results questioning downsizing in moderately luminous AGN with $42 < \log L_X < 44$ (Aird et al. 2012). In general, the presence of both downsizing and occupation fraction complicates estimates of either parameter alone. For example, a downsizing-enhanced detectability of SMBHs down the mass scale could bias high an estimate of the occupation fraction that presumes a uniform Eddington fraction. The slope of the dependence of L_X upon M_{star} is primarily sensitive to the higher mass galaxies, most of which are X-ray detected, but could potentially be influenced by partial occupation in lower mass galaxies. To date occupation fraction and downsizing have not been simultaneously constrained.

To investigate the occupation fraction of SMBHs and simultaneously their Eddington rates across the mass scale, we consider the measurable distribution of X-ray

⁸ Enriched gas cannot directly collapse to produce a massive seed (e.g., Ferrara et al. 2013).

⁹ The masses of central black holes in dwarf galaxies are difficult to measure precisely, but the following examples are likely near or above our adopted definitional threshold for a SMBH.

¹⁰ AGN Multiwavelength Survey of Early-Type Galaxies

luminosities as a function of host galaxy stellar mass. Motivated by prior studies we take $\log L_X$ to be a linear function of $\log M_{\text{star}}$ but allow for significant intrinsic scatter; see Figure 1a. It is assumed that the degree of intrinsic scatter remains constant across the mass scale and we note as a caveat that this is observationally uncertain. The L_X – M_{star} correlation is observationally truncated by the sensitivity limit of the AMUSE surveys, which is $\log L_X \simeq 38.3 \text{ erg s}^{-1}$. A decreasing occupation fraction toward lower M_{star} would result in a portion of galaxies not following the L_X – M_{star} correlation but presenting instead as non-detections, since they would lack an SMBH to generate X-ray emission.

We consider occupation fractions bounded by $f_{\text{occ}} \simeq 0$ for $M_{\text{star}} < 10^7 M_\odot$ and $f_{\text{occ}} \simeq 1$ for $M_{\text{star}} > 10^{10} M_\odot$. The probability of hosting an SMBH is taken to be

$$0.5 + 0.5 \times \tanh(2.5^{[8.9 - \log M_{\text{star},0}] \log \frac{M_{\text{star}}}{M_{\text{star},0}}) \quad (1)$$

This simple functional form was selected because it is smooth and spans a wide range of plausible possibilities, and in particular includes both the light “stellar death” and the heavy “direct collapse” competing seed formation models (from van Wassenhove et al. 2010; Volonteri 2010) as illustrated in Greene (2012; see their Figure 2). We show this parameterization in Figure 1 for $7.5 < \log M_{\text{star},0} < 10.2$, which correspond to occupation fractions between 98% and 2% for galaxies with $M_{\text{star}} < 10^{10} M_\odot$. Note that here and throughout occupation fractions are derived from a given $M_{\text{star},0}$ value by applying the probabilities in Figure 1b to the AMUSE M_{star} distribution in Figure 1c, and that by construction even models with a low occupation fraction (always quoted, we emphasize, for galaxies with $M_{\text{star}} < 10^{10} M_\odot$) produce nearly 100% SMBH occupation in high-mass galaxies.

The relationships we assume throughout between M_{star} , L_X , and the SMBH occupation fraction are illustrated in Figure 1. The simulated sample of 10000 galaxies (the colored points in the top panel) has M_{star} drawn from an unevenly-weighted sum of four Gaussians constructed to empirically match the mass distribution of the AMUSE surveys.¹¹ The expected nuclear X-ray luminosities where an SMBH is present are calculated from the L_X – M_{star} correlation, here given by the best-fit model to the full AMUSE sample (the solid black trend line), but with significant intrinsic scatter to match that observed. Next, each of the simulated galaxies is assigned an SMBH based on the choice of $M_{\text{star},0}$; i.e., the high $M_{\text{star},0}$ red curve in panel (b) populates only the high mass galaxies shown by the red points in panel (a), whereas the intermediate $M_{\text{star},0}$ blue curve populates the high mass galaxies down to the intermediate mass galaxies shown by the red through blue points, and finally the low $M_{\text{star},0}$ green curve populates nearly all galaxies down to dwarfs shown by the red through green points. Panel (c) shows the total simulated M_{star} distribution, which by construction matches the AMUSE sample, and uses the same color coding to illustrate the progression in occupation fraction as parameterized by $M_{\text{star},0}$. The conversion from simulated to observed L_X then results

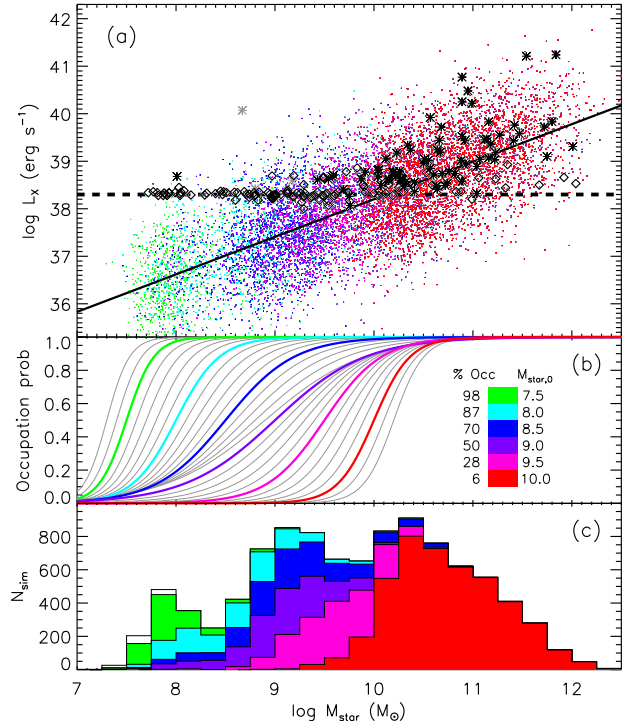


Figure 1. (a) X-ray luminosity versus stellar mass. AMUSE early-type galaxies are plotted as black stars (X-ray detections); gray stars are star-forming galaxies excluded from the clean sample defined in §3) or as diamonds (upper limits). The horizontal dashed black line is the typical AMUSE sensitivity limit. The solid black trend line shows the best-fit relation for the full sample and the colored points are a random realization of this model. (b) Illustration of the parameterization used to model different occupation fractions. The colored lines show $\log M_{\text{star},0}$ values and their consequent occupation fraction (for galaxies with $\log M_{\text{star}} < 10$) as given in the legend; see text for details. (c) Distribution of M_{star} simulated from a sum of four Gaussians to match the AMUSE dataset; the histograms show occupied galaxies color-coded as in (b).

from imposing a sensitivity threshold, such as the horizontal dotted black line in panel (a) from AMUSE, and changing L_X to an upper limit (with a value narrowly scattered around the threshold) for all galaxies that either lack an SMBH or else have an SMBH emitting below the detection sensitivity.

We modified the Bayesian linear regression code of Kelly (2007) to fit for the SMBH occupation fraction (i.e., $M_{\text{star},0}$) while simultaneously determining L_X as a function of M_{star} . The primary difference between the method of Kelly (2007) and our extension is that the method of Kelly (2007) would model the distribution of L_X at fixed M_{star} as a single normal distribution, whereas we here model the distribution of $L_X|M_{\text{star}}$ as a mixture of a normal distribution and a delta function centered at an extremely small value of L_X , with the mixing weights as a function of M_{star} given by the occupation fraction at that M_{star} . Specifically, we assume

$$p(\log L_X | \log M_{\text{star}}) = f_{\text{occ}}(M_{\text{star}}) N(\log L_X | \alpha + \beta \log M_{\text{star}}, \sigma^2) + (1.0 - f_{\text{occ}}(M_{\text{star}})) \delta(\log L_X + 9999) \quad (2)$$

¹¹ The central $\log M_{\text{star}}$ values, standard deviations, and fractional weights for the four Gaussians are (7.9, 9.2, 10.3, 11.0), (0.2, 0.5, 0.3, 0.5), and (0.10, 0.43, 0.20, 0.27), respectively; the KS-test agreement with the full AMUSE distribution is $p = 0.996$.

where $N(x|\mu, \sigma^2)$ denotes a normal distribution with mean μ and variance σ^2 as a function of x , and α, β , and σ^2 denote the intercept, slope, and variance in the intrinsic scatter of the $\log L_X$ – $\log M_{\text{star}}$ relationship, and $\delta(\cdot)$ is the Dirac delta function.

In order to obtain samples of $\log M_{\text{star},0}$, α , β , and σ^2 from their posterior distribution, we used an extension of the Gibbs sampler of Kelly (2007). In our Gibbs sampler we introduce a latent indicator variable, I_i , where $I_i = 1$ if the i^{th} galaxy has a black hole in it and $I_i = 0$ otherwise. For all sources with X-ray detections $I_i = 1$ and is considered known, while for those with upper limits I_i is unknown. For those sources with unknown I_i we update their values of I_i at each stage of the Gibbs sampler by drawing from a Bernoulli distribution with probability

$$p(I_i = 1 | L_{X,i}, M_{\text{star},i}, \alpha, \beta, \sigma^2, M_{\text{star},0}) = \frac{\Phi\left(\frac{\log L_{X,i} - \alpha - \beta \log M_{\text{star},i}}{\sigma}\right)}{\left[1 - (1 + \Phi\left(\frac{\log L_{X,i} - \alpha - \beta \log M_{\text{star},i}}{\sigma}\right))f_{\text{occ}}(M_{\text{star},0})\right]^{-1}} \quad (3)$$

where $\Phi(\cdot)$ denotes the cumulative distribution function of the standard normal distribution. Given these new values of I_i we can then update $M_{\text{star},0}$ using a Metropolis update in combination with the conditional posterior

$$p(\log M_{\text{star},0} | I_1, \dots, I_n) = \prod_{i=1}^n [f_{\text{occ}}(M_{\text{star},0})]^{I_i} [1 - f_{\text{occ}}(M_{\text{star},0})]^{1-I_i}. \quad (4)$$

The rest of the Gibbs sampler proceeds as in Kelly (2007).

The parameter $\log M_{\text{star},0}$ is restricted to be greater than 7.5 since any values below 7.5 already produce near 100% occupation fraction. As with the original `linmix_err` IDL routine, measurement errors, intrinsic scatter, and upper limits are incorporated, and the independent variable distribution is approximated as a sum of Gaussians. The four parameters of interest in our model are the intercept, slope, and intrinsic scatter of the $L_X(M_{\text{star}})$ relation as well as $\log M_{\text{star},0}$, which gives the occupation fraction for galaxies below $M_{\text{star}} = 10^{10} M_{\odot}$. The best-fit preferred parameter values are taken as the median of 5000 (thinned from 50000, retaining every tenth) draws from the posterior distribution and quoted errors correspond to 1σ uncertainties.

3. RESULTS FROM THE AMUSE SURVEYS

Stellar masses and X-ray luminosities for the AMUSE Virgo and Field sample were previously published in G10 and M12a.¹² As described in those works, the detected nuclear *Chandra* X-ray sources are point-like and located at the projected optical center of their galaxy, to within the optical and X-ray astrometric and centroid uncertainties. We determine more precise stellar masses for some of the AMUSE galaxies using archival and newly obtained *HST* data, including Cycle 19 two-color *HST* ACS imaging of Field galaxies (Baldassare et al. 2014; B14

¹² NGC 5077 ($d > 30$ Mpc) and NGC 4627 (atypically deep serendipitous coverage) are here removed from the Field sample.

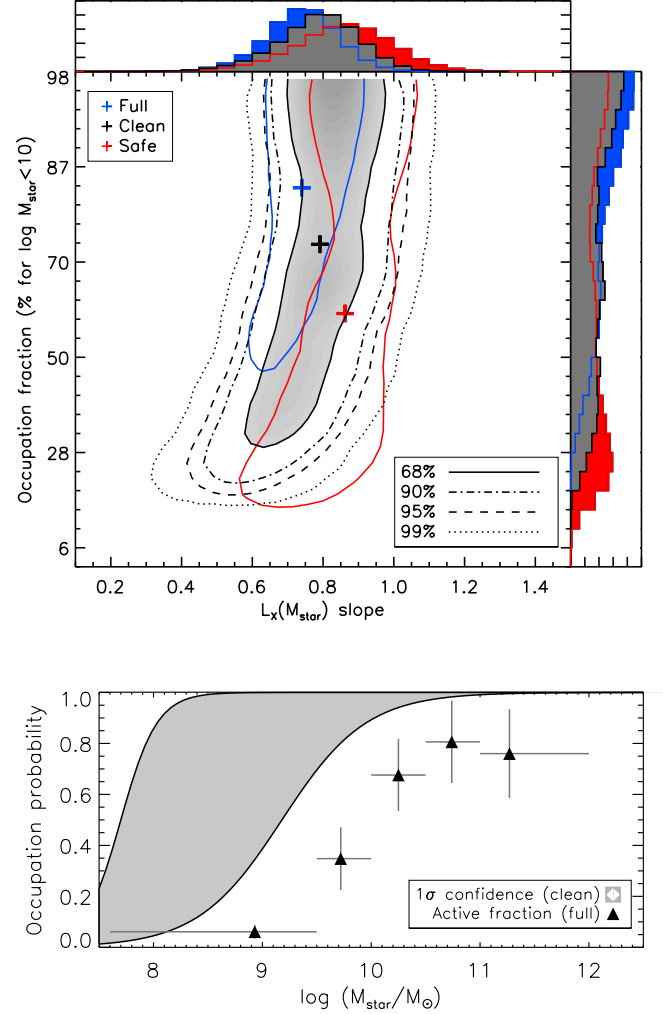


Figure 2. *Top:* Preferred model for the AMUSE dataset, for the clean, full, and safe samples (black, blue, and red; see text for details). The median values from the posterior probability are marked with crosses, and the histograms show the marginalized distributions. Joint 68%, 90%, 95%, and 99% confidence contours are plotted for the clean sample. *Bottom:* Permitted occupation probability (1σ confidence) as a function of M_{star} for the clean AMUSE dataset, along with the active fraction from the full sample. The active fraction provides a lower limit for the occupation fraction, and the full sample provides the highest detection fraction.

hereafter). Two Field galaxies, NGC 3928 (described as a starburst by Carollo et al. 1997) and NGC 3265, show spiral arms in *HST* imaging and are removed. We also cautiously choose to set aside VCC 1857 and VCC 1828 from the Virgo sample, as these two galaxies have irregular and late types, respectively, in HyperLeda despite their arguably elliptical appearance. The “full” AMUSE sample then consists of 197 early-type galaxies of which 81 (or 41%) have X-ray detections.

The distances to the Virgo galaxies were assumed as 16.4 Mpc in G10 and the distances to the Field galaxies were calculated from their redshifts in M12a. We here (and in B14) make use of slightly more accurate distances, specifically taking distances to Virgo galaxies from Mei et al. (2007) and distances to Field galax-

ies from non-redshift measurements given in HyperLeda where available. The stellar masses and X-ray luminosities are adjusted from G10 and M12a using these more accurate distances (with *HST*-derived M_{star} values for some Field galaxies taken from B14); the resulting full AMUSE Virgo and Field combined sample properties are given in Table 1. While the properties for several individual galaxies are improved in accuracy, this adjustment has only a tiny statistical impact on the overall sample, with a median change to M_{star} and L_X of 0.02 dex (standard deviation of 0.11 dex).

We next generate a “clean” sample by removing three galaxies for which optical or UV *HST* imaging shows irregular or clumpy morphology and colors suggestive of recent ($<100\text{--}300$ Myr) star formation. From the Field sample, NGC 855 and ESO 540–014 display clumpy structure with blue colors (a spectrum of the latter indicates high star-formation rates rather than the literature Seyfert 2 classification; Amy Reines, private communication). From the Virgo sample, VCC 1499 has archival *HST* UV imaging that is suggestive of galaxy-wide star-formation, and it is identified as post-starburst by Gavazzi et al. (2001). These three galaxies all have detectable nuclear X-ray emission, but their optical morphologies and blue colors indicate X-ray contamination from high-mass X-ray binaries is possible. The clean sample then contains 194 galaxies of which 78 have X-ray detections.¹³

Finally, we generate a “safe” sample by correcting for potential contamination of the nuclear X-ray emission due to low-mass X-ray binaries (LMXBs). The probability of contamination of the nuclear X-ray emission from LMXBs enclosed by the projected *Chandra* point spread function, within the $d < 30$ Mpc volume-limited AMUSE sample, is generally negligible for non-nucleated galaxies (see G10 for details; for context, $1''$ corresponds to projected 50/100/150 pc at distances of 10/20/30 Mpc). For galaxies hosting a nuclear star cluster, the probability of contamination is greater and is conservatively estimated using a globular cluster X-ray luminosity function (G10; B14). Taking into account the measured nuclear X-ray luminosities, the probability of LMXB contamination is $\gtrsim 50\%$ in four Virgo galaxies (VCC 1883, VCC 784, VCC 1250, and VCC 1283 have contamination probabilities of 100%, 51%, 100%, and 45%; G10). From the *HST*-covered Field sample NGC 3384, NGC 1172, and NGC 2970 have non-negligible contamination probabilities (B14); NGC 3384 is known from stellar dynamics to have an SMBH with a mass of $\sim 1.8 \times 10^7 M_\odot$ (Gebhardt et al. 2000) so we flag NGC 1172 and NGC 2970. NGC 1331 is the only additional Field galaxy known to have both a NSC and a central X-ray source, but it has a $<5\%$ probability of LMXB contamination. From among the Field galaxies that have a detected nuclear X-ray source but lack *HST* coverage, about three more are statistically expected to contain nuclear star clusters that could generate LMXB contamination. An example is NGC 3522 with $\log M_{\text{star}}/M_\odot < 10$ and a moderate $\log L_X = 38.8$, and we randomly chose two others from NGC 2778, NGC 3457, NGC 3641, NGC 4283,

NGC 1370, or PGC 1206166 in four ways, producing four slightly different versions of a safe sample. The X-ray luminosities for the nine flagged galaxies are converted to limits for the safe sample, which then still contains 194 galaxies but with 69 now considered to be X-ray detections. The four slightly different versions of the safe sample produce formally consistent fitting results, although the median occupation fraction is lower if PGC 1206166 with $\log M_{\text{star}}/M_\odot = 8.0$ is considered contaminated (illustrating the importance of every X-ray detection in the dwarf galaxy regime).

The safe sample provides a deliberately cautious approach to LMXB contamination. Both the Virgo and Field samples include several galaxies with nuclear star clusters that are not detected in X-rays; for example, from the Field NGC 1340 and NGC 1426 have calculated probabilities of $\sim 10\%$ for having a central LMXB with L_X greater than the AMUSE sensitivity. Because the probability of hosting a nuclear star cluster increases to lower stellar mass (as does the profile cuspieness, centrally partially offsetting the absolute decrease in M_{star}), the potentially contaminated galaxies all have $M_{\text{star}} < 3 \times 10^{10} M_\odot$. (The Field sample has relatively more low-mass galaxies, nucleated galaxies, and potentially contaminated galaxies, but the frequency of nuclear star clusters after accounting for stellar mass is similar to that in Virgo; B14). The impact of conservatively correcting for LMXB contamination is to reduce slightly the inferred occupation fraction and to increase slightly the slope. The most accurate representation of the AMUSE dataset likely lies between the clean and safe samples, probably closer to the former given the conservative LMXB correction.

A low percentage of X-ray detections in low-mass galaxies arises from some combination of a low occupation fraction, a steep $L_X(M_{\text{star}})$ slope, and small intrinsic scatter. For the AMUSE sample, the overall detection fraction is 41% (36% after accounting for potential LMXB contamination); most of these detections (84%, or slightly higher after LMXB correction) are in galaxies with $\log M_{\text{star}} > 10$, and only 1–2% of galaxies with $\log M_{\text{star}} < 9$ have nuclear X-ray detections. For illustration, similar distributions can be produced for slopes of 1.0 with occupation fractions between 50% and 100% and intrinsic scatter of 0.7 dex, or for slopes of 0.7 with 50% occupation fraction and intrinsic scatter of 0.5 dex. However, flatter slopes < 0.4 that match the overall detection fraction necessarily overpredict the proportion of detections in low-mass galaxies, and occupation fractions of $< 20\%$ underpredict that same ratio.

The results of applying this modeling framework to the AMUSE dataset are shown in Figure 2. The posterior distributions of the slope and the occupation fraction for the full, clean, and safe AMUSE samples are plotted as confidence contours and marginalized histograms. (To illustrate the spread in the safe samples we plot all four versions combined.) The slope is relatively well-constrained even with occupation fraction as a free parameter (0.74 ± 0.10 , 0.79 ± 0.12 , or 0.86 ± 0.14 for the full, clean, and safe samples). For the clean sample, the slope has a negligible ($\lesssim 0.05$) probability of being < 0.5 or > 1.0 . However, the occupation fraction is only loosely constrained; the probability distribution extends from 30% to 100% ($p = 0.34, 0.46$ for occupation $> 87\%$,

¹³ We reconfirm using the clean sample the marginally significant finding from M12b that the Field galaxies tend to be X-ray brighter than their Virgo counterparts.

< 70%). Only occupation fractions of <20% are securely ruled out by our data. (Recall that dynamical SMBH mass limits for M33 and NGC 205 argue against a 100% occupation fraction). Figure 2, bottom, shows the 1σ confidence region for the occupation probability as a function of M_{star} , along with the lower limits provided by the X-ray active fraction. The significant uncertainties prevent a definitive discrimination between formation mechanisms.¹⁴

The preferred $L_X(M_{\text{star}})$ slope of ~ 0.7 – 0.8 for the full or clean AMUSE samples supports downsizing in these weakly accreting SMBHs, albeit with respect to M_{star} rather than inferred M_{BH} as given in G10 and M12b. (We used simulations to confirm that an input universal Eddington ratio distribution would produce preferred slopes $\simeq 1$ with our methodology.) While dynamical measurements of M_{BH} in these galaxies are not available, a typical scaling of $M_{\text{BH}} \sim M_{\text{bulge}}^{1.12 \pm 0.06}$ (Häring & Rix 2004) would suggest this downsizing effect is similar or perhaps slightly more pronounced with black hole mass rather than host galaxy stellar mass.¹⁵ Additional dynamical measurements (such as that in NGC 404; Seth et al. 2010; see also Neumayer & Walcher 2012) are required to confirm the intriguing apparent tendency for M_{BH} in lower mass galaxies to fall below the extrapolation of the Häring & Rix (2004) relation (see Greene 2012 and references therein). It seems unlikely that $M_{\text{BH}}/M_{\text{star}}$ could increase for dwarfs such that $\log L_X$ could scale linearly with $\log M_{\text{BH}}$.

We emphasize that these results are derived from early-type galaxies, and insofar as SMBH seeding and growth is linked to bulge properties rather than stellar mass (e.g., Beifiori et al. 2012) they may not apply to late-type or irregular galaxies.

4. ASSESSING UNCERTAINTIES AND FUTURE PROSPECTS FROM SIMULATIONS

To assess prospects for improving constraints upon the occupation fraction with future surveys, we use the Bayesian linear regression fitting to investigate the impact of the limiting sensitivity and the sample size upon the parameter errors.

The distribution of L_X versus M_{star} is only subtly changed by partial occupation fraction for the AMUSE sensitivity limit (Figure 3, right column), because most of the impacted low-mass galaxies would already have X-ray luminosities precluding detection. To examine the impact of the sensitivity limit (as well as to validate our modeling techniques), we also consider an artificially increased sensitivity of $\log L_{X,\text{limit}} = 36.3$ erg s⁻¹, two orders of magnitude below that for the AMUSE surveys. This contrived model usefully illustrates the impact of downsizing and partial occupation (Figure 3, left).

We verified that arbitrary input parameters are cleanly recovered (with correct statistical uncertainties) in simulations given an artificially increased sensitivity of $\log L_{X,\text{limit}} = 36.3$ erg s⁻¹. Recall that for these simula-

¹⁴ Since both pathways are theoretically viable and presumably operate at some level, definitive identification of the dominant seeding mode would not rule out that some supermassive black holes formed from alternative mechanisms.

¹⁵ For most of these early-type galaxies $M_{\text{bulge}} \simeq M_{\text{star}}$; also, applying a bulge-to-total correction would make the downsizing more extreme.

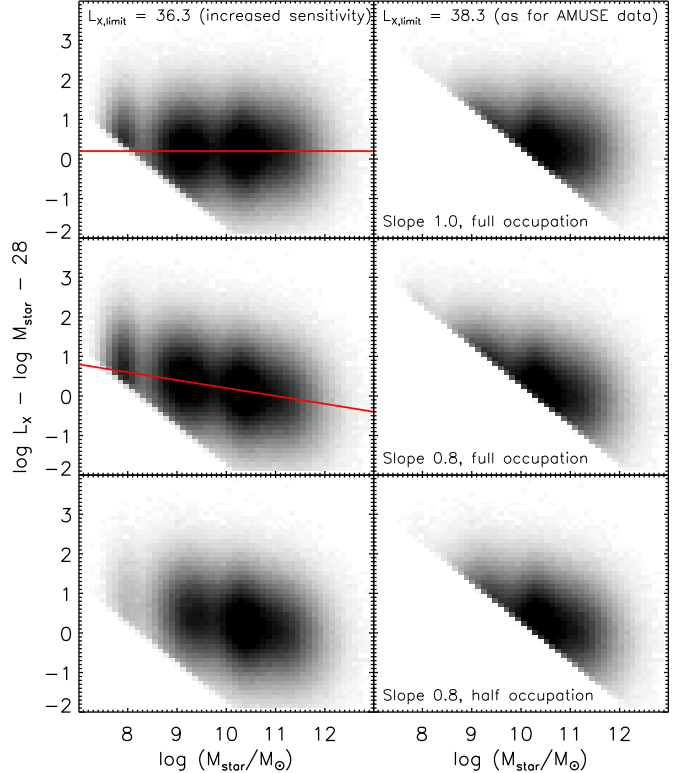


Figure 3. Simulated distribution of X-ray detected objects for an artificially increased sensitivity of $L_X = 36.3$ (left column) and for the AMUSE sensitivity of $L_X = 38.3$ (right column). 10^6 points are binned in a 50-by-50 tiling, and the density is plotted in grayscale with squareroot scaling. The top and middle rows are for full occupation with slopes of 1.0 (uniform Eddington efficiency) and 0.8 (downsizing), while the bottom row is for an occupation fraction of $\sim 50\%$ for $M_{\text{star}} < 10^{10} M_\odot$, again with a downsizing 0.8 slope.

tions M_{star} values are drawn from a sum of four Gaussians which empirically matches the AMUSE distribution, L_X is computed from M_{star} for a given correlation, and then the occupation fraction is enforced following the probability curve for a given $M_{\text{star},0}$ value (Figure 1b) and objects then lacking an SMBH are mandated to be X-ray upper limits. Some examples of fitting these simulations are provided in Figure 4 for input slopes of 0.4, 0.7, and 1.0 and occupation fractions of 15%, 50%, and 85%. The sample size was fixed to 200 objects, and the simulated points were varied by an intrinsic $L_X(M_{\text{star}})$ scatter of 0.7 dex for 100 realizations of each model. The resulting uncertainties on both parameters are modest even with only 200 points (and consistent with the output errors from the code). Unfortunately, even the outstanding *Chandra* PSF is not sufficient to overcome the rapid rise in the luminosity function of low-mass X-ray binaries and so contamination becomes impossible to avoid below the AMUSE sensitivity limit of $\log L_X \sim 38.3$ erg s⁻¹. With higher spatial resolution the total projected stellar mass enclosed in an X-ray extraction aperture, and correspondingly the likelihood of contamination, could be decreased. To achieve a $20\times$ improvement in sensitivity down to $\log L_{X,\text{limit}} \sim 37.0$ erg s⁻¹, for galaxies of stellar

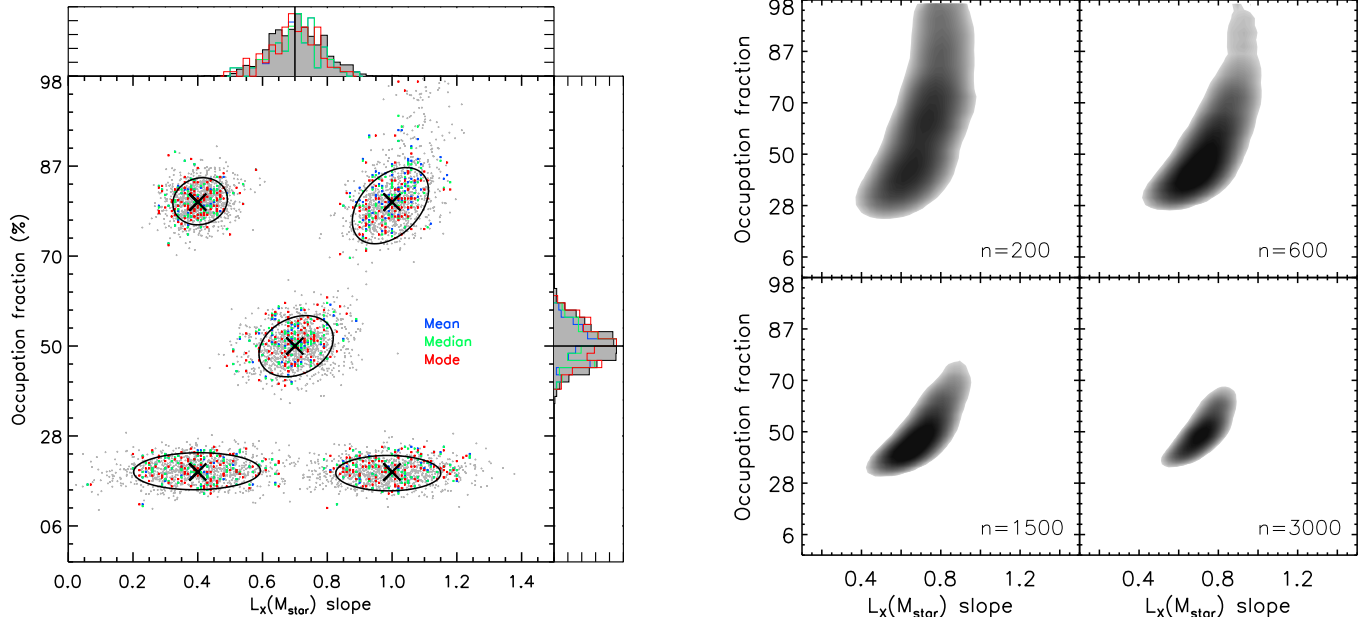


Figure 4. *Left:* Illustration of the uncertainties in the slope and occupation fraction for simulations from different input models for an artificially increased sensitivity $\log L_{X,\text{limit}} = 36.3 \text{ erg s}^{-1}$. The input parameters are cleanly recovered with only 200 simulated data points. *Right:* Illustration of the uncertainties in the slope and occupation fraction for simulations with differing sample sizes, as indicated, for sensitivity $\log L_{X,\text{limit}} = 38.3 \text{ erg s}^{-1}$ matching the AMUSE dataset.

mass $\sim 10^9 M_\odot$ lying within 30 Mpc (with effective radii of $\sim 15''$) a resolution of $\sim 0.05''$ would be necessary to limit potential contamination to $< 10\%$ in a given X-ray nuclear detection. The inclusion of X-ray variability or spectral measurements (or other activity indicators, such as radio emission) could weaken this requirement.

The impact of increasing the sample size is also shown in Figure 4, for $\log L_{X,\text{limit}} = 38.3 \text{ erg s}^{-1}$ as for the AMUSE dataset. For these simulations new objects are added at the AMUSE M_{star} distribution probabilities but weighted by a factor of two for $\log M_{\text{star}} < 10$; the uncertainties on the occupation fraction converge more quickly when smaller galaxies are preferentially targeted. With only 600 total objects, the statistical errors on the occupation fraction permit clean differentiation between full and half occupation, and with 1500 objects the occupation can be fixed to $\pm 15\%$. If the slope or intrinsic scatter were known (for example, from theoretical arguments) rather than fit, far fewer objects would be required to obtain such constraints. There are good prospects for combining the AMUSE samples with new coverage (e.g., of the outer Fornax cluster), or with archival coverage of low-mass galaxies serendipitously present in existing very deep *Chandra* observations of M87 in Virgo or 3C 84 in Perseus. Here ultra-compact dwarf galaxies, which may contain SMBHs and have undergone tidal stripping (Mieske et al. 2013; Seth et al. 2014), could be included.

5. DISCUSSION AND FUTURE APPLICATIONS

Our simultaneous fitting of the SMBH occupation fraction and the scaling of nuclear X-ray luminosity with stellar mass constrains SMBHs to be present in $> 20\%$ of early-type galaxies with $M_{\text{star}} < 10^{10} M_\odot$ and suggests the dependence of $\log L_X$ upon $\log M_{\text{star}}$ has a slope of $\sim 0.7\text{--}0.8$. This work provides promising if inconclusive information on the local SMBH occupation fraction and

also supports a downsizing trend in low-level SMBH activity.

The highly sub-Eddington objects that make up the AMUSE dataset are expected to feature radiatively inefficient accretion flows (RIAFs). Bondi accretion of even the limited gas provided by stellar winds (Volonteri et al. 2011) near the nuclei of early-type galaxies would predict greater X-ray luminosities than observed; the efficiency as well as the accretion rate must be low in these objects (Soria et al. 2006; Ho 2009). Either an advection-dominated accretion flow (e.g., Di Matteo & Fabian 1997; Narayan et al. 1998) or an outflow/jet component (e.g., Soria et al. 2006; Plotkin et al. 2012) is required. In general, the efficiency in these hot flows is theoretically expected to decrease toward lower accretion rates (Yuan & Narayan 2014 and references therein). Although the Bondi radius is directly resolved by *Chandra* in deep observations of NGC 3115, the temperature profile is inconsistent with simple RIAF models (Wong et al. 2014). Fueling of a RIAF by steady-state stellar winds may be supplemented by intermittent processes such as tidal disruption, or by gradual stripping of central stars (e.g., MacLeod et al. 2013). While we cannot constrain the physical mechanism responsible for the observed X-ray emission, the simplest explanation for downsizing in low-level SMBH activity would be that the relative rate of accretion is higher in smaller galaxies, with a fixed low efficiency. We reiterate that the downsizing we identify here is restricted to low-level SMBH activity and may not apply to AGNs.

The methodology we use here is flexible and could also be applied to deep surveys of AGN. For example, the 4 Ms CDFS contains active galactic nuclei including to relatively modest $M_{\text{star}} \lesssim 3 \times 10^9 M_\odot$ (Schramm & Silverman 2013; Schramm et al. 2013) and at low levels of

activity (Young et al. 2012) as well as normal galaxies at cosmological distances (Lehmer et al. 2012), and opens substantial additional volume albeit at lower sensitivity. We provide an illustration of applying this general technique to simulated deep field galaxies in Figure 5, and are pursuing this approach in Greene et al. (in preparation).

In this higher L_X regime we populate X-ray luminosities drawing from a uniform Eddington ratio distribution with a power-law slope of -0.65 as in Aird et al. (2012), assuming $\log M_{\text{BH}} = \log M_{\text{star}} - 2.8$. For a hypothetical combined CDFS+CDFN+AEGISXD sample with a typical detection sensitivity of $\log L_X \simeq 40$ out to $z < 0.4$, we expect about 15000 $z < 0.4$ galaxies (estimated from Cardamone et al. 2010; Xue et al. 2010) of which ~ 300 or 2% should host X-ray AGNs (estimated from Xue et al. 2010, 2011; Lehmer et al. 2012). We confirmed with an artificially large sample that the distribution of X-ray detections (color gradients in Figure 5) can be used to infer the occupation fraction. For example, the percentages of X-ray AGNs in hosts with $\log M_{\text{star}} < 9.5$ is 11.9% with full occupation versus 6.1% with half occupation. This is statistically distinguishable at 99% confidence for the expected $\simeq 300$ AGNs (black crosses in Figure 5) if the other model parameters are known or fixed by theory; full versus half occupation predicts 37 versus 17 X-ray AGNs in hosts with $\log M_{\text{star}} < 9.5$). This test will increase in power with the upcoming deeper CDFS exposure.

We are also refining our measurement of occupation fraction within the AMUSE sample through incorporating the influence of large-scale environment upon low-level SMBH activity. The scaled nuclear X-ray luminosities of early-type galaxies apparently decrease from isolated to group to cluster environments (M12a,b). This may reflect greater quantities of cold gas in field galaxies (e.g., Oosterloo et al. 2010), for example due to reduced stripping relative to their cluster counterparts. Cold accretion has been inferred to be relevant to low-level SMBH activity from studies of brightest cluster galaxies (Russell et al. 2013) and dust (Martini et al. 2013), and AGNs preferentially inhabit gas-rich galaxies (Vito et al. 2014). The recent tentative finding that nuclear star clusters in massive early type galaxies are bluer in the field (B14) implies that field nuclear star clusters formed at lower metallicities and/or experienced more recent star formation, relative to cluster counterparts; this in turn suggests that cold gas can eventually filter down to the central regions where it is available (either directly or via enhanced star formation and stellar winds) to be heated and inefficiently accreted onto the central SMBH. We are continuing to investigate the impact of Mpc-scale densities using new *Chandra* observations of early-type galaxies located within cosmic voids. However, the analysis presented here is not biased because the slopes of the $L_X - M_{\text{star}}$ relation are consistent between the AMUSE-Field and AMUSE-Virgo samples (M12b); instead, the uncertainties are potentially slightly inflated. Including any environmental dependence, once quantified at high significance, will helpfully decrease the scatter in the $L_X(M_{\text{star}})$ relation in the combined AMUSE dataset.

Additional multiwavelength information will provide better understanding of both individual objects and of the overall population (e.g., the distribution of galaxies showing radio, or optical, indications of nuclear activity; Reines et al. 2013). New dynamical mass measurements

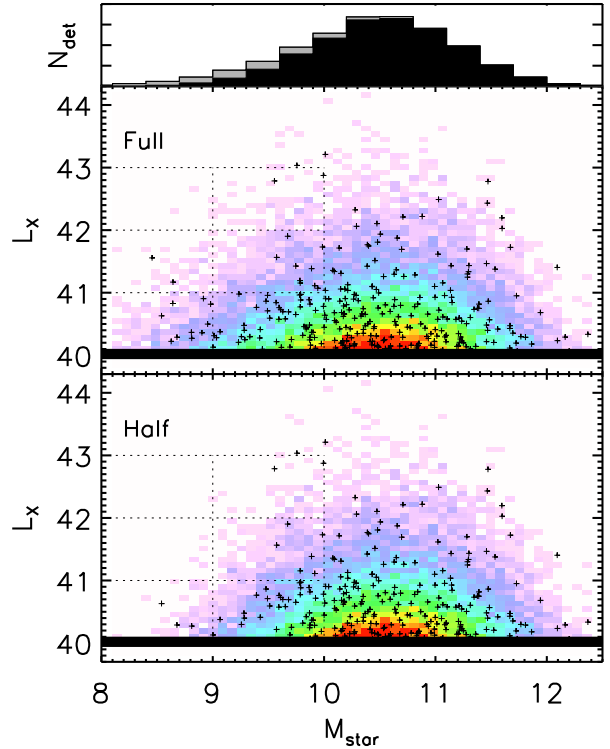


Figure 5. Distribution of AGN X-ray detections for mock deep field catalogs with 50% and 100% occupation fractions for $M_{\text{star}} < 10^{10} M_{\odot}$. The colors indicate detection density with the black crosses a realization with 15000 total galaxies and ~ 300 X-ray AGN, ± 20 depending on the occupation fraction. The top histogram shows X-ray detected AGN for half (black) and full (gray) occupation.

with a 30m class telescope would help clarify the mass distribution of SMBHs in smaller galaxies, providing a complementary probe of black hole birth and growth (van Wassenhove et al. 2010). In this context it is interesting that no galaxies with $M_{\text{star}} < 10^{10} M_{\odot}$ (without stripping; Seth et al. 2014) are yet known with confirmed $M_{\text{BH}} > 10^6 M_{\odot}$. Tidal disruption transients, particularly from white dwarfs, can provide complementary insight into lower-mass SMBHs (Clausen & Eracleous 2011; MacLeod et al. 2014). Pairing observational advances with increasingly sophisticated theoretical models will help discriminate between models of seed formation.

We thank Andy Fabian, Rich Plotkin, Amy Reines, Claudia Scarlata, and Anil Seth for helpful discussions, and an anonymous referee for constructive comments. This work was supported in part by Chandra Award Number 11620915, by the National Science Foundation under grant no. NSF PHY11-25915 and by NASA through grant HST-GO-12591.01 from the Space Telescope Science Institute, which is operated by AURA, Inc., under NASA contract NAS 5-26555. JHW acknowledges support by the National Research Foundation of Korea (NRF) grant funded by the Korea government (MEST; No. 2012-006087).

REFERENCES

- Aird, J., Coil, A. L., Moustakas, J., et al. 2012, *ApJ*, 746, 90
- Allen, S. W., Dunn, R. J. H., Fabian, A. C., Taylor, G. B., & Reynolds, C. S. 2006, *MNRAS*, 372, 21
- Agarwal, B., Dalla Vecchia, C., Johnson, J. L., Khochfar, S., & Paardekooper, J.-P. 2014, *MNRAS*, 443, 648
- Baldassare, V. F., Gallo, E., Miller, B. P., et al. 2014, *ApJ*, 791, 133
- Balmaverde, B., Baldi, R. D., & Capetti, A. 2008, *A&A*, 486, 119
- Beifiori, A., Courteau, S., Corsini, E. M., & Zhu, Y. 2012, *MNRAS*, 419, 2497
- Begelman, M. C. 2010, *MNRAS*, 402, 673
- Cano-Díaz, M., Maiolino, R., Marconi, A., et al. 2012, *A&A*, 537, L8
- Cardamone, C. N., van Dokkum, P. G., Urry, C. M., et al. 2010, *ApJS*, 189, 270
- Carollo, C. M., Stiavelli, M., de Zeeuw, P. T., & Mack, J. 1997, *AJ*, 114, 2366
- Clausen, D., & Eracleous, M. 2011, *ApJ*, 726, 34
- Croton, D. J., Springel, V., White, S. D. M., et al. 2006, *MNRAS*, 365, 11
- Davies, M. B., Miller, M. C., & Bellovary, J. M. 2011, *ApJ*, 740, L42
- Dijkstra, M., Ferrara, A., & Mesinger, A. 2014, *MNRAS*, 442, 2036
- Di Matteo, T., & Fabian, A. C. 1997, *MNRAS*, 286, L50
- Ferrara, A., Haardt, F., & Salvaterra, R. 2013, *MNRAS*, 434, 2600
- Ferrara, A., Salvadori, S., Yue, B., & Schleicher, D. 2014, *MNRAS*, 443, 2410
- Feruglio, C., Maiolino, R., Piconcelli, E., et al. 2010, *A&A*, 518, L155
- Gallo, E., Treu, T., Jacob, J., Woo, J.-H., Marshall, P. J., & Antonucci, R. 2008, *ApJ*, 680, 154
- Gallo, E., Treu, T., Marshall, P. J., Woo, J.-H., Leipski, C., & Antonucci, R. 2010, *ApJ*, 714, 25
- Gavazzi, G., Zibetti, S., Boselli, A., et al. 2001, *A&A*, 372, 29
- Gebhardt, K., Bender, R., Bower, G., et al. 2000, *ApJ*, 539, L13
- Gebhardt, K., Lauer, T. R., Kormendy, J., et al. 2001, *AJ*, 122, 2469
- Greene, J. E. 2012, *Nature Communications*, 3,
- Gültekin, K., et al. 2009, *ApJ*, 698, 198
- Häring, N., & Rix, H.-W. 2004, *ApJ*, 604, L89
- Ho, L. C. 2009, *ApJ*, 699, 626
- Jiang, Y.-F., Greene, J. E., Ho, L. C., Xiao, T., & Barth, A. J. 2011, *ApJ*, 742, 68
- Johnson, J. L., Whalen, D. J., Li, H., & Holz, D. E. 2013, *ApJ*, 771, 116
- Kuo, C. Y., Asada, K., Rao, R., et al. 2014, *arXiv:1402.5238*
- Lapi, A., Raimundo, S., Aversa, R., et al. 2014, *ApJ*, 782, 69
- Latif, M. A., Schleicher, D. R. G., Schmidt, W., & Niemeyer, J. 2013a, *MNRAS*, 433, 1607
- Latif, M. A., Schleicher, D. R. G., Schmidt, W., & Niemeyer, J. C. 2013b, *MNRAS*, 436, 2989
- Lehmer, B. D., Xue, Y. Q., Brandt, W. N., et al. 2012, *ApJ*, 752, 46
- Liu, G., Zakamska, N. L., Greene, J. E., Nesvadba, N. P. H., & Liu, X. 2013, *MNRAS*, 436, 2576
- Lupi, A., Colpi, M., Devecchi, B., Galanti, G., & Volonteri, M. 2014, *MNRAS*, 442, 3616
- MacLeod, M., Ramirez-Ruiz, E., Grady, S., & Guillochon, J. 2013, *ApJ*, 777, 133
- MacLeod, M., Goldstein, J., Ramirez-Ruiz, E., Guillochon, J., & Samsing, J. 2014, *ApJ*, 794, 9
- Madau, P., Haardt, F., & Dotti, M. 2014, *ApJ*, 784, L38
- Martini, P., Dicken, D., & Storchi-Bergmann, T. 2013, *ApJ*, 766, 121
- McConnell, N. J., & Ma, C.-P. 2013, *ApJ*, 764, 184
- Mei, S., Blakeslee, J. P., Côté, P., et al. 2007, *ApJ*, 655, 144
- Merritt, D., Ferrarese, L., & Joseph, C. L. 2001, *Science*, 293, 1116
- Mieske, S., Frank, M. J., Baumgardt, H., et al. 2013, *A&A*, 558, A14
- Miller, B., Gallo, E., Treu, T., & Woo, J.-H. 2012a, *ApJ*, 747, 57
- Miller, B., Gallo, E., Treu, T., & Woo, J.-H. 2012b, *ApJ*, 745, L13
- Mortlock, D. J., Warren, S. J., Venemans, B. P., et al. 2011, *Nature*, 474, 616
- Narayan, R., Mahadevan, R., Grindlay, J. E., Popham, R. G., & Gammie, C. 1998, *ApJ*, 492, 554
- Natarajan, P., & Volonteri, M. 2012, *MNRAS*, 422, 2051
- Natarajan, P. 2014, *General Relativity and Gravitation*, 46, 1702
- Neumayer, N., & Walcher, C. J. 2012, *Advances in Astronomy*, 2012,
- Nguyen, D. D., Seth, A. C., Reines, A. E., et al. 2014, *ApJ*, 794, 34
- Oosterloo, T., Morganti, R., Crocker, A., et al. 2010, *MNRAS*, 409, 500
- Pellegrini, S. 2010, *ApJ*, 717, 640
- Petri, A., Ferrara, A., & Salvaterra, R. 2012, *MNRAS*, 422, 1690
- Plotkin, R. M., Markoff, S., Kelly, B. C., Körding, E., & Anderson, S. F. 2012, *MNRAS*, 419, 267
- Reines, A. E., Sivakoff, G. R., Johnson, K. E., & Brogan, C. L. 2011, *Nature*, 470, 66
- Reines, A. E., Greene, J. E., & Geha, M. 2013, *ApJ*, 775, 116
- Reines, A. E., Plotkin, R. M., Russell, T. D., et al. 2014, *ApJ*, 787, L30
- Russell, H. R., McNamara, B. R., Edge, A. C., et al. 2013, *MNRAS*, 432, 530
- Salvaterra, R., Haardt, F., Volonteri, M., & Moretti, A. 2012, *A&A*, 545, L6
- Schramm, M., & Silverman, J. D. 2013, *ApJ*, 767, 13
- Schramm, M., Silverman, J. D., Greene, J. E., et al. 2013, *ApJ*, 773, 150
- Seth, A. C., Cappellari, M., Neumayer, N., et al. 2010, *ApJ*, 714, 713
- Seth, A. C., van den Bosch, R., Mieske, S., et al. 2014, *Nature*, 513, 398
- Shankar, F., Weinberg, D. H., & Miralda-Escudé, J. 2013, *MNRAS*, 428, 421
- Soltan, A. 1982, *MNRAS*, 200, 115
- Soria, R., Graham, A. W., Fabbiano, G., et al. 2006, *ApJ*, 640, 143
- Sun, A.-L., Greene, J. E., Impellizzeri, C. M. V., et al. 2013, *ApJ*, 778, 47
- Taylor, P., & Kobayashi, C. 2014, *MNRAS*, 442, 2751
- Treu, T., Woo, J.-H., Malkan, M. A., & Blandford, R. D. 2007, *ApJ*, 667, 117
- Valluri, M., Ferrarese, L., Merritt, D., & Joseph, C. L. 2005, *ApJ*, 628, 137
- van Wassenhove, S., Volonteri, M., Walker, M. G., & Gair, J. R. 2010, *MNRAS*, 408, 1139
- Vestergaard, M., & Osmer, P. S. 2009, *ApJ*, 699, 800
- Vito, F., Maiolino, R., Santini, P., et al. 2014, *arXiv:1403.7966*
- Volonteri, M., & Natarajan, P. 2009, *MNRAS*, 400, 1911
- Volonteri, M. 2010, *A&A Rev.*, 18, 279
- Volonteri, M., Dotti, M., Campbell, D., & Mateo, M. 2011, *ApJ*, 730, 145
- Volonteri, M. 2012, *Science*, 337, 544
- Volonteri, M., & Bellovary, J. 2012, *Reports on Progress in Physics*, 75, 124901
- Whalen, D. J., & Fryer, C. L. 2012, *ApJ*, 756, L19
- Willott, C. J., Albert, L., Arzoumanian, D., et al. 2010, *AJ*, 140, 546
- Wong, K.-W., Irwin, J. A., Shcherbakov, R. V., et al. 2014, *ApJ*, 780, 9
- Woo, J.-H., Treu, T., Barth, A. J., et al. 2010, *ApJ*, 716, 269
- Woo, J.-H., Schulze, A., Park, D., et al. 2013, *ApJ*, 772, 49
- Xue, Y. Q., Brandt, W. N., Luo, B., et al. 2010, *ApJ*, 720, 368
- Xue, Y. Q., Luo, B., Brandt, W. N., et al. 2011, *ApJS*, 195, 10
- Young, M., Brandt, W. N., Xue, Y. Q., et al. 2012, *ApJ*, 748, 124
- Yuan, F., & Narayan, R. 2014, *arXiv:1401.0586*
- Yuan, W., Zhou, H., Dou, L., et al. 2014, *ApJ*, 782, 55

Table 1
Combined AMUSE Virgo and Field sample of early-type galaxies

Name	V/F	Distance (Mpc)	Method	$\log M_{\text{star}}$ (M_{\odot})	$\log L_X$ (erg s^{-1})	Notes
VCC 1226	V	17.1	M07	12.0	<38.5	
VCC 731	V	23.3	M07	12.0	39.3	
VCC 881	V	16.8	M07	11.9	<38.7	
VCC 1316	V	17.2	M07	11.8	41.2	
VCC 763	V	18.4	M07	11.8	39.8	
VCC 1978	V	17.3	M07	11.8	39.1	
NGC 1407	F	28.6	HL	11.7	39.7	
VCC 798	V	17.9	M07	11.7	<38.5	
IC 1459	F	29.0	HL	11.5	41.2	
NGC 5322	F	30.9	HL	11.5	39.6	
NGC 2768	F	22.2	HL	11.4	39.8	
NGC 0720	F	27.4	HL	11.4	39.4	
NGC 5846	F	24.7	HL	11.3	<38.9	
NGC 3923	F	20.0	HL	11.3	<38.4	
VCC 1632	V	15.8	M07	11.3	39.5	
NGC 7507	F	24.8	HL	11.2	39.2	
NGC 3640	F	26.8	HL	11.2	<38.6	
VCC 1903	V	14.9	M07	11.2	39.0	
NGC 1332	F	22.7	HL	11.2	39.4	
NGC 4125	F	23.7	HL	11.2	39.1	
NGC 4494	F	16.7	HL	11.2	39.8	
NGC 3610	F	32.5	HL	11.1	39.5	
NGC 3193	F	33.7	HL	11.1	39.5	
NGC 3585	F	19.9	HL	11.1	39.0	
VCC 575	V	22.1	M07	11.1	<38.6	
NGC 0821	F	23.3	HL	11.0	38.9	
NGC 4636	F	14.1	HL	11.0	38.3	
VCC 1535	V	16.3	HL	11.0	<38.2	
NGC 4036	F	21.1	HL	11.0	40.2	
NGC 1052	F	17.5	HL	10.9	40.5	
NGC 5576	F	25.2	HL	10.9	38.9	
NGC 5838	F	19.5	z	10.9	39.4	
VCC 2092	V	16.1	M07	10.9	38.6	
NGC 4291	F	32.2	HL	10.9	39.5	
NGC 4278	F	18.5	HL	10.9	40.2	
NGC 4203	F	15.0	HL	10.9	40.8	
NGC 5638	F	26.1	HL	10.9	<38.4	
VCC 1154	V	16.1	M07	10.9	39.0	
NGC 1340	F	20.6	HL	10.9	<38.6	
VCC 759	V	17.0	M07	10.8	<38.4	
VCC 1030	V	16.8	M07	10.8	38.7	
NGC 4697	F	12.2	HL	10.8	38.8	
VCC 1231	V	15.3	M07	10.7	38.5	
NGC 3379	F	11.3	HL	10.7	38.5	
NGC 3115	F	9.6	HL	10.7	38.7	
NGC 5845	F	32.7	HL	10.7	39.7	
VCC 1025	V	22.4	M07	10.7	39.2	
NGC 5831	F	26.9	HL	10.7	39.4	
NGC 1439	F	26.4	HL	10.6	39.2	
VCC 1062	V	15.3	M07	10.6	38.4	
VCC 1692	V	17.1	M07	10.6	38.5	
VCC 2095	V	16.4	Vir	10.6	38.7	
NGC 1426	F	23.3	HL	10.6	<38.5	
VCC 1664	V	15.8	M07	10.6	39.9	
NGC 5582	F	28.2	HL	10.6	38.9	
VCC 1938	V	17.5	M07	10.6	39.0	
VCC 1279	V	17.0	M07	10.5	<38.8	
VCC 685	V	14.9	HL	10.5	39.0	
NGC 4648	F	25.4	z	10.5	39.0	
VCC 1883	V	16.6	M07	10.4	38.4	NSC + X-ray
NGC 3384	F	9.4	HL	10.4	38.6	NSC + X-ray
VCC 1720	V	16.3	M07	10.4	<38.5	
VCC 944	V	16.0	M07	10.4	<38.5	
VCC 369	V	15.8	M07	10.4	39.2	
NGC 6017	F	29.5	HL	10.3	39.3	
VCC 2000	V	15.0	M07	10.3	38.6	
NGC 1172	F	22.0	HL	10.3	38.5	NSC + X-ray
VCC 654	V	14.7	M07	10.3	<38.4	
NGC 3377	F	10.4	HL	10.3	38.6	
VCC 828	V	17.9	M07	10.3	<38.7	
VCC 778	V	17.8	M07	10.3	38.6	
VCC 784	V	15.8	M07	10.3	38.6	NSC + X-ray
VCC 1250	V	17.6	M07	10.3	38.8	NSC + X-ray
VCC 1242	V	15.6	M07	10.2	<38.5	

Table 1 — *Continued*

Name	V/F	Distance (Mpc)	Method	$\log M_{\text{star}}$ (M_{\odot})	$\log L_X$ (erg s^{-1})	Notes
VCC 355	V	15.4	M07	10.2	38.7	
NGC 4742	F	15.3	HL	10.2	39.2	
NGC 2778	F	22.7	HL	10.2	38.7	No HST; NSC?
NGC 3457	F	20.5	HL	10.2	38.8	No HST; NSC?
VCC 1630	V	16.1	M07	10.2	<38.3	
VCC 1327	V	18.3	M07	10.2	38.8	
VCC 1913	V	17.4	M07	10.2	<38.5	
VCC 1619	V	15.5	M07	10.2	38.6	NSC + X-ray
VCC 1283	V	17.4	M07	10.2	38.6	NSC + X-ray
VCC 1303	V	16.8	M07	10.1	<38.3	
IC 1729	F	19.5	z	10.1	39.0	
VCC 698	V	18.7	M07	10.1	<38.5	
VCC 1537	V	15.8	M07	10.1	38.5	
NGC 4283	F	15.6	HL	10.1	38.8	No HST; NSC?
VCC 1321	V	15.4	M07	10.1	<38.3	
ESO 576-076	F	23.6	z	10.1	<38.4	
UGC 07767	F	27.5	HL	10.0	38.7	
NGC 3641	F	26.4	HL	10.0	38.8	No HST; NSC?
VCC 1146	V	16.4	M07	10.0	<38.3	
NGC 3522	F	25.5	HL	9.9	38.8	No HST; NSC?
VCC 1475	V	16.6	M07	9.9	<38.4	
VCC 1125	V	16.4	Vir	9.9	<38.5	
VCC 1261	V	18.1	M07	9.9	<38.5	
VCC 1178	V	15.8	M07	9.9	38.6	
NGC 3073	F	33.4	HL	9.8	<38.9	
NGC 4121	F	24.8	z	9.8	38.1	
NGC 1331	F	22.9	HL	9.8	38.3	NSC + X-ray
UGC0 5955	F	22.4	z	9.7	<38.4	
VCC 9	V	17.1	M07	9.7	<38.3	
VCC 571	V	23.8	M07	9.7	<38.8	
VCC 1297	V	16.3	M07	9.7	38.4	
VCC 437	V	17.1	M07	9.6	<38.4	
VCC 1087	V	16.7	M07	9.6	<38.3	
VCC 2048	V	16.4	Vir	9.6	<38.3	
NGC 1370	F	13.2	z	9.6	38.7	No HST; NSC?
NGC 2970	F	25.9	z	9.6	38.7	NSC + X-ray
VCC 1422	V	15.3	M07	9.5	<38.2	
NGC 1097A	F	16.7	z	9.5	<38.1	
PGC 056821	F	27.0	z	9.5	38.6	
VCC 856	V	16.8	M07	9.5	<38.3	
VCC 1695	V	16.5	M07	9.5	<38.3	
VCC 1431	V	16.1	M07	9.5	<38.6	
VCC 1861	V	16.1	M07	9.5	<38.3	
VCC 1192	V	16.1	HL	9.5	<38.7	
VCC 1910	V	16.1	M07	9.5	<38.3	
VCC 1871	V	15.5	M07	9.4	<38.2	
VCC 2019	V	17.1	M07	9.4	<38.4	
VCC 1355	V	16.9	M07	9.4	38.6	NSC + X-ray
VCC 140	V	16.4	M07	9.4	<38.3	
VCC 751	V	15.8	M07	9.4	<38.3	
VCC 543	V	15.7	M07	9.4	<38.2	
VCC 1512	V	18.4	M07	9.3	<38.3	
NGC 4308	F	12.0	z	9.3	<38.0	
VCC 1833	V	16.2	M07	9.3	<38.2	
VCC 1528	V	16.3	M07	9.3	<38.3	
VCC 200	V	18.2	M07	9.3	<38.5	
PGC 3119319	F	23.6	z	9.3	<38.1	
PGC 042748	F	15.5	z	9.3	<38.3	
VCC 1545	V	16.8	M07	9.2	<38.3	
VCC 1075	V	16.1	M07	9.2	<38.3	
VCC 538	V	22.9	M07	9.2	<38.7	
VCC 1440	V	16.0	M07	9.2	<38.2	
NGC 0855	F	9.6	HL	9.2	38.6	Starforming
IC 0225	F	21.9	z	9.1	<38.3	
VCC 1185	V	16.9	M07	9.1	<38.4	
VCC 1407	V	16.8	M07	9.1	<38.4	
NGC 7077	F	17.8	z	9.1	<38.3	
VCC 1627	V	15.6	M07	9.1	<38.3	
VCC 1993	V	16.5	M07	9.0	<38.3	
VCC 1488	V	16.4	Vir	9.0	<38.3	
VCC 21	V	16.4	Vir	9.0	<38.3	
VCC 1779	V	16.4	Vir	9.0	<38.3	
VCC 1049	V	16.0	M07	9.0	<38.2	
PGC 132768	F	20.1	z	9.0	<38.3	
VCC 1199	V	16.0	HL	9.0	<38.3	

Table 1 — *Continued*

Name	V/F	Distance (Mpc)	Method	$\log M_{\text{star}}$ (M_{\odot})	$\log L_X$ (erg s^{-1})	Notes
VCC 1895	V	15.8	M07	9.0	<38.2	
VCC 2050	V	15.8	M07	9.0	<38.2	
VCC 230	V	17.8	M07	9.0	<38.7	
VCC 1661	V	15.8	M07	9.0	<38.2	
VCC 1743	V	17.6	M07	9.0	<38.3	
NGC 5099	F	19.0	z	8.9	<38.3	
VCC 1539	V	16.9	M07	8.9	<38.3	
PGC 1210284	F	26.6	z	8.8	<38.4	
VCC 33	V	15.1	M07	8.8	<38.2	
VCC 1886	V	16.4	Vir	8.8	<38.3	
VCC 1948	V	16.4	Vir	8.8	<38.3	
VCC 1499	V	16.4	Vir	8.8	38.4	Starforming
PGC 1209872	F	26.6	z	8.8	<38.3	
VCC 1826	V	16.2	M07	8.8	<38.3	
PGC 740586	F	19.0	z	8.7	<38.2	
PGC 028305	F	23.0	z	8.7	<38.3	
VCC 1489	V	16.5	HL	8.7	<38.3	
PGC 1242097	F	27.7	z	8.7	<38.4	
ESO 540-014	F	22.4	z	8.7	40.1	Starforming
PGC 042173	F	23.0	z	8.6	<38.3	
PGC 064718	F	9.7	z	8.6	<38.2	
PGC 042737	F	26.6	z	8.6	<38.4	
PGC 1216386	F	26.6	z	8.5	<38.3	
PGC 1230503	F	27.7	z	8.5	<38.4	
PGC 030133	F	17.2	z	8.5	<38.3	
6dF J2049400-324154	F	24.2	z	8.4	<38.4	
PGC 1202458	F	25.4	z	8.4	<38.3	
SDSS J145828.64+01323	F	23.0	z	8.3	<38.3	
SDSS J150812.35+01295	F	23.6	z	8.3	<38.3	
PGC 042724	F	10.9	z	8.2	<38.3	
SDSS J150907.83+00432	F	25.4	z	8.1	<38.4	
PGC 1179083	F	25.4	z	8.1	<38.4	
PGC 042596	F	12.6	z	8.0	<38.3	
PGC 3097911	F	19.0	z	8.0	<38.3	
PGC1 35659	F	15.5	z	8.0	<38.5	
PGC 1206166	F	26.6	z	8.0	38.7	No HST; NSC?
SDSS J150233.03+01560	F	25.4	z	8.0	<38.3	
SDSS J150100.85+01004	F	26.6	z	7.9	<38.3	
PGC 1223766	F	24.2	z	7.9	<38.3	
PGC 135818	F	14.9	z	7.9	<38.3	
PGC 135829	F	20.7	z	7.9	<38.3	
PGC 1217593	F	17.2	z	7.9	<38.3	
SDSS J145944.77+02075	F	22.4	z	7.9	<38.3	
PGC 042454	F	12.6	z	7.9	<38.3	
PGC 085239	F	20.7	z	7.8	<38.3	
SDSS J150033.02+02134	F	20.1	z	7.8	<38.3	
PGC 1192611	F	23.6	z	7.8	<38.4	
PGC 043421	F	16.7	z	7.7	<38.3	

Note. — Column 1: Object name from HyperLeda, or VCC for Virgo galaxies; Column 2: V = Virgo, F = Field; Column 3: Adopted distance in Mpc; Column 4: Distance method, with M07 = from Mei et al. (2007), HL = non-redshift distance in HyperLeda, z = calculated from redshift, and Vir = assumed 16.4 Mpc for Virgo; Column 5: Stellar mass calculated as in G10 and M12a for these distances; Column 6: X-ray luminosity calculated as in G10 and M12a for these distances; Column 7: Starforming = clumps of star formation present, removed from clean sample; NSC + X-ray = dual nuclear star cluster and nuclear X-ray source; No HST; NST? = lacks high-resolution ACS *HST* coverage but might be a candidate for LMXB contamination of the nuclear X-ray emission if a NSC is present. See text for details of construction of the safe sample.